DOI: 10.1039/b902811k

Re-investigation of the spin crossover phenomenon in the ferrous complex $[Fe(HB(pz)_3)_2]$†

Lionel Salmon,*[ab] Gábor Molnár,[ab] Saioa Cobo,[ab] Pascal Oulié,[ab] Michel Etienne,[ab] Tarik Mahfoud,[abc] Philippe Demont,[d] Akira Eguchi,[e] Hiroshi Watanabe,[e] Koichiro Tanaka[e] and Azzedine Bousseksou*[ab]

The temperature dependence of the magnetic susceptibility, optical reflectivity and electrical conductivity of $[Fe(HB(pz)_3)_2]$ (pz = pyrazolyl) revealed irreversible changes in the material during the low-spin to high-spin transition when the "as-prepared" sample was heated above ~400 K for the first time. During this first heating sequence, the initially fine powder sample became coarse, and its crystal structure changed from tetragonal to monoclinic. Single-crystals of the monoclinic form suitable for X-ray analysis could be isolated after the first thermal cycle, and their structure was resolved in the $P2_1/n$ ($Z = 4$) space group. Successive cooling and heating cycles did not lead to further modification of the crystal structure, and the temperature dependence of the physical properties remained invariable. Remarkably, the electrical conductivity of the sample measured at 293 K dropped from 6.1×10^{-8} to 2.1×10^{-11} S m^{-1} following the first thermal cycle—suggesting possible applications of this material in read-only memory devices (ROM).

1. Introduction

Coordination complexes containing various substituted poly(1-pyrazolyl)borate ligands have been intensively investigated since the pioneering work of Trofimenko.[1] Iron and cobalt derivatives, among several other possible complexes, have received particular attention because their spin state equilibrium is highly sensitive to ligand substitution.[2] The ferrous complex formed with the hydrotris(1-pyrazolyl)borate ligand, $[Fe(HB(pz)_3)_2]$ (**1**), where pz = pyrazolyl, is one of the most studied complexes of this family (Fig. 1). In this thermochromic complex, the iron(II) ions undergo a thermally-induced spin crossover between their $^1A_1$ low-spin (LS) and $^5T_2$ high-spin (HS) electronic configurations in the 300–450 K temperature range. This high temperature spin crossover (SCO) behavior was first revealed by optical spectroscopy[3] and confirmed later by magnetic susceptibility, Mössbauer and infrared spectroscopic studies.[4,5] Interestingly, the thermal spin transition curve recorded during the first heating differs drastically from the successive thermal cycles. Grandjean *et al.*[5] explained this rather unusual observation by shattering the initially microcrystalline sample into a fine powder, which they observed on a melting point stage during the first heating. Indeed, it is well-established that the spin crossover phenomenon is very sensitive to grinding of the sample.[6,7] These mechanical treatments induce various defects in the crystal lattice, leading to more and more gradual and incomplete transition curves. Moreover, it was reported in many instances that single-crystals of spin crossover complexes break apart when going through the spin transition. This phenomenon occurs due to the important volume change which accompanies these transitions.[8] However, crystal fracture leads in general only to slight changes in physical properties. In this context, we have found only one well-documented literature report on self-grinding phenomena in a spin crossover system. Miyazaki *et al.*[9] revealed that single-crystals of

[a] *CNRS, Laboratoire de Chimie de Coordination, 205 route de Narbonne, Toulouse, France*
[b] *Université de Toulouse, UPS, INPT, LCC, 31077 Toulouse, France. E-mail: boussek@lcc-toulouse.fr, frsalmon@lcc-toulouse.fr*
[c] *School of Science and Engineering, Al Akhawayn University in Ifrane, 53000 Ifrane, Morocco*
[d] *Laboratoire de Physique des Polymères-CIRIMAT, CNRS UMR-5085, Université Toulouse III, 118 Route de Narbonne, 31062 Toulouse Cedex, France*
[e] *Department of Physics, Graduate School of Science, Kyoto University, Sakyo-ku, Kyoto 606-8502, Japan*

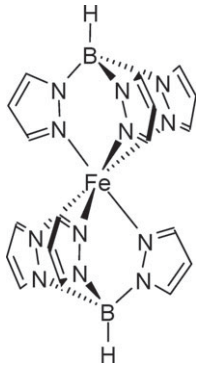

Fig. 1 The schematic structure of $[Fe(HB(pz)_3)_2]$ (**1**).

[Fe(DAPP)(abpt)]$(ClO_4)_2$ (DAPP = bis(3-aminopropyl)(2-pyridylmethyl)amine and abpt = 4-amino-3,5-bis(pyridin-2-yl)-1,2,4-triazole) gradually disintegrate upon thermal cycling, and this morphological change is accompanied by a continuous variation of the physical properties. The occurrence of such a violent self-grinding effect in **1** therefore appears rather surprising. For this reason, we repeated and extended previous studies on this compound by investigating its physical properties and crystal structure in a wide temperature range. These new data confirm most of the observations made by Grandjean *et al.*,[5] but refute their interpretation of the observed magnetic behavior. In the course of this study, interesting and unexpected electrical properties of **1** were also been uncovered, of possible relevance for the technological application of this compound.

2. Experimental section

Synthesis

Hydrotris(1-pyrazolyl)borate ligand[10] and the corresponding $[Fe(HB(pz)_3)_2]$ iron(II) complex[5] were synthesized according to experimental procedures reported in the literature. The $[Fe(HB(pz)_3)_2]$ complex was sublimed at 463 K in a vacuum (*ca.* 0.1 Torr) prior to use, and either a microcrystalline clear violet powder or small single-crystals (depending on the sublimation conditions) were obtained. Elemental analysis calculated for $[Fe(HB(pz)_3)_2]$ (481.91 g mol^{-1}): calc. C, 44.86; N, 34.88; H, 4.18; found C, 44.61; N 34.53; H, 4.09%.

Physical properties

Magnetic susceptibility measurements were carried out at heating and cooling rates of 2 K min^{-1} in a 2 T magnetic field by means of a Quantum Design MPMS2 SQUID magnetometer. The experimental data were corrected for the diamagnetic contribution. AC conductivity data were recorded in the two-probe geometry using a Novocontrol BDS 4000 broadband dielectric spectrometer coupled to a Quatro Cryosystem. Frequency sweeps (10^{-2}–10^6 Hz) were carried out isothermally in the 220–445 K temperature range. Diffuse reflectance measurements were performed using a halogen lamp, a heating and cooling stage (Linkam), and a Princeton Instruments monochromator and CCD camera system (InSight100A).

Thermal analysis

Differential thermal analysis and thermogravimetric (DTA-TG) data were acquired simultaneously using a SETARAM 92–16.18 thermal analyzer. Differential scanning calorimetry (DSC) analysis was carried out on a Netzsch DSC 204 instrument under helium purging gas (20 cm^3 min^{-1}) at a heating/cooling rate of 10 K min^{-1}. Temperature and enthalpy (ΔH) were calibrated using the melting transition of standard materials (Hg, In, Sn).

Microscope observations

The morphology of samples was observed under an Olympus BX51 optical microscope equipped with a DP12 digital camera. Images of the crystals were recorded during the heating and cooling cycles through the window of a Linkam THMS600 variable temperature stage, and also at room temperature before and after a thermal cycle using a $\times 5$ or $\times 20$ objective lens, respectively.

X-Ray crystallography

A Panalytical MPD XPert Pro powder diffractometer and an Antoon Paar TTK 450 Chamber were used to acquire variable temperature powder diffractograms between room temperature and 453 K. The extraction of peak positions for indexing and cell refinement were performed with the fitting program DICVOL, available in the PC software package Highscore + supplied by Panalytical. Single-crystal X-ray diffraction (XRD) data were collected at room temperature and 420 K with monochromatic Mo-K_α radiation ($\lambda = 0.71073$) using an Xcalibur (Oxford Diffraction) diffractometer. A total of 12 676 reflections were collected at room temperature, of which 3218 unique reflections were used for the structure determination. The second collection at 420 K was formed from 13 117 measured reflections, 3411 of which independent reflections were used for the hypothesis and refinement. DIRDIF92[11] was used for the structure solutions, SHELXL-97[12] for the refinements and PLATON[13] for structure analysis. The final R factor (with $I > 2\sigma(I)$) had values of 0.0431 and 0.0501 for the 298 and 420 K measurements, respectively. Crystallographic data are given in Table 1. The temperature dependence of the unit cell parameters between 298 and 423 K was determined using a KAPPA-CCD-Enraf-Nonius diffractometer.

3. Results and discussion

Physical properties

Fig. 2 shows the temperature dependence of the product of the molar magnetic susceptibility (χ_M) and the temperature (T) for a powder sample of **1**. The magnetic properties of $Fe[HB(pz)_3]_2$ were reported earlier in refs. 4 and 5. The results we obtained are quite similar to these reports. In our case, the $\chi_M T$ product of **1** (''as-prepared'') exhibited a gradual increase from 0.07 cm^3 mol^{-1} K at 300 K to 1.21 cm^3 mol^{-1} K at 405 K, then an abrupt increase to 2.40 cm^3 mol^{-1} K at 410 K and finally a gradual increase to 2.80 cm^3 mol^{-1} K at 450 K. On the contrary, upon cooling, the $\chi_M T$ product gradually decreased to 0.197 cm^3 mol^{-1} K at 300 K. In agreement with

Table 1 Crystallographic data for **1**†

	T = 180 K	T = 298 K	T = 420 K
Chemical formula		$C_{18}H_{20}N_{12}B_2Fe$	
M_w		481.9	
a/Å	9.900(2)	9.9390(7)	9.8400(6)
b/Å	17.020(3)	17.0720(16)	17.6210(19)
c/Å	12.890(3)	12.9410(14)	13.3150(14)
β (°),	96.53(3)	96.658(7)	97.068(7)
V/Å^3	2157.8(8)	2181.0(3)	2291.2(4)
Z	4	4	4
Space group	$P2_1/n$	$P2_1/n$	$P2_1/n$
r_{calc}/g cm^{-3}	1.483	1.468	1.397
μ/cm^{-1}	0.734	0.726	0.691
R factor	0.027	0.0409	0.0501
Weighted R factor	0.0673	0.0804	0.0642

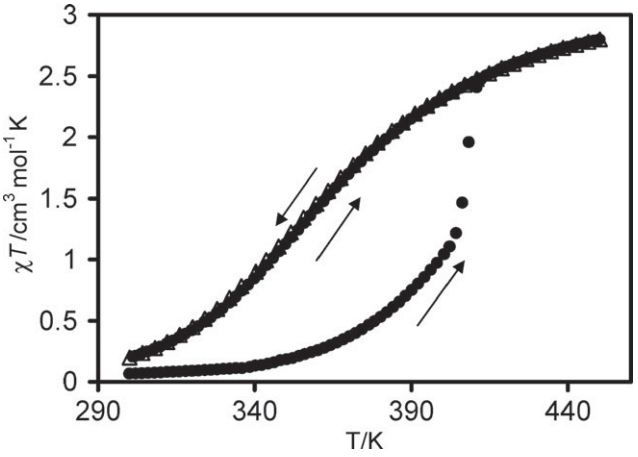

Fig. 2 The temperature dependence of the $\chi_M T$ product of **1** upon two successive thermal cycles (first cycle: closed circles, second cycle: open triangles).

the initial report of Hutchinson *et al.*,[4] the magnetic susceptibility displayed an apparent hysteresis only for the first thermal cycle. For all subsequent cooling and heating treatments, the magnetic properties retraced the initial cooling curve and not the initial heating curve. The temperature at which the sharp and irreversible transition was observed in our sample is different somewhat from previous reports (410 K *vs.* 390 K[5]). One should recognize, however, that the initial state (*i.e.* the freshly sublimated sample) of this transition is thermodynamically unstable, and obviously no characteristic transition temperature exists for such a system, since the transformation from the metastable to the stable phase depends not only on the temperature, but also on the time.

The spin crossover in **1** is also accompanied by spectacular color changes (see ESI†). At room temperature, the "as-prepared" sample has a violet color, which fades when it is heated to 470 K. Remarkably, when the sample is cooled back to room temperature, its visual aspect appears very different from the initial one. At the end of the first cycle, the initially pale-violet fine microcrystalline powder becomes coarse, leading to a deeper color and a more brilliant aspect. We have also carried out a microscopic observation of these morphological changes, as shown in Fig. 3. The optical microscope clearly shows that the sample is composed of small, needle-like crystallites of a few μm in size before the first thermal cycle (Fig. 3a), while it reveals the presence of well-defined single-crystals having various sizes up to a few hundred μm after the first cycle (Fig. 3b). Indeed, the *in situ* observation during the first heating process (see ESI†) demonstrates clearly that at 430 K large single-crystals can already grow within a few minutes from the initially fine powder. This recrystallisation process is certainly related to the fact that around 430 K, the sublimation of the sample slowly begins. These observations are not in agreement with those of Grandjean *et al.*,[5] who actually reported the opposite process, *i.e.*, the disintegration of the sample at the end of the first thermal cycle. In order to obtain more quantitative details of the optical changes, we have acquired variable temperature diffuse reflectance spectra of **1** in the 400–900 nm range. Fig. 4(a) displays the reflectivity spectra at different temperatures during the first two thermal cycles. The spectra are plotted as $-\log(R_{sig}/R_{ref})$, where R_{sig}/R_{ref} is the normalized reflectance signal, since this quantity is almost proportional to the absorbance of the sample, provided that the scattering coefficient is wavelength-independent. The reflectance spectrum of the sample at room temperature is characterized by an intense absorption band centered around 530 nm—responsible for the violet color of the compound—which was assigned to the $^1A_{1g} \rightarrow {}^1T_{1g}$ ligand-field absorption of the LS molecules.[14] When the temperature increases the intensity of this band decreases due to the transformation of the singlet LS ground state to the quintet HS state, leading to the bleaching of the samples. During the first heating cycle one can also observe a

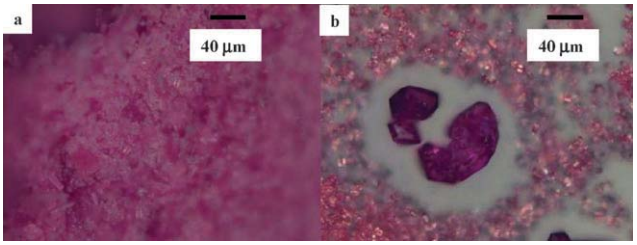

Fig. 3 Microscope images recorded at 295 K displaying the typical aspect of the same sample a: before and b: after the first thermal cycle.

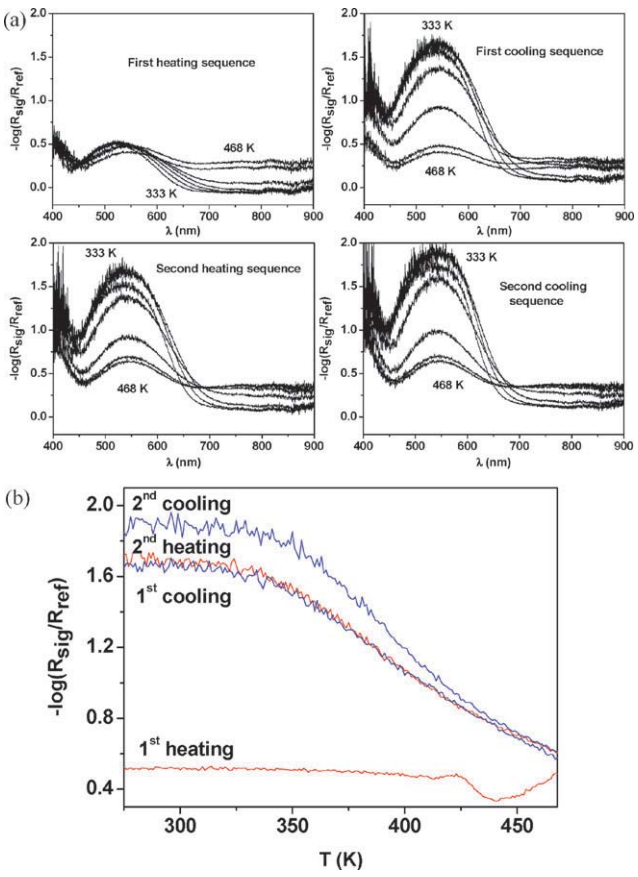

Fig. 4 (a) Diffuse reflectance spectra of **1** recorded at various temperatures during the first two thermal cycles. (b) Temperature dependence of the reflectivity of **1** (recorded at 530 nm) upon two successive thermal cycles.

rather abrupt change of the reflectance signal around 420 K (Fig. 4(b)), which can be straightforwardly correlated with the discontinuous change observed in the magnetic measurements. Moreover, the first heating cycle differs significantly from the subsequent cooling and heating cycles, which nearly follow the same trace. These findings are in good agreement with the report of Grandjean *et al.*[5] However, Fig. 4(a) and 4(b) very clearly reveal that the reflectance of the "as-prepared" sample at 300 K (*i.e.*, in the pure LS state) is not the same as that of the thermally cycled sample. The observed enhancement of the singlet absorption band is, of course, not related to any change of absorption coefficient, but occurs due to the change of the scattering coefficient, which can be traced back to the altered sample granularity (Fig. 3).

Besides the magnetic and optical properties, the SCO phenomenon is known to be accompanied by changes of the electrical properties as well. Actually, most SCO complexes are highly insulating, and pertinent information can be obtained by determining their (quasi-static) dielectric constant.[15] We therefore measured the complex impedance of a powder sample of **1** (placed between two gold-plated brass electrodes) over a large frequency and temperature range. Quite surprisingly we noticed that the conductivity of the sample was relatively high, $\sim 6 \times 10^{-8}$ S m^{-1}, at room temperature. This observation was confirmed on two independently-synthesized batches, proving that it is not due to adventitious contamination but is an inherent property of this complex. Fig. 5(a) displays the frequency dependence of the real part, σ'(f), of the complex conductivity σ^*(f), recorded at representative temperatures during the first heating cycle. At each temperature, one can distinguish low and high frequency regions. In both regions, the conductivity exhibits only a slight frequency dependence, but the high frequency part of the spectrum is characterized by a higher conductivity. The critical frequency, f_c, which separates the low and high frequency regions, increases continuously with increasing temperature from *ca.* 1 Hz to 10 kHz between 243 and 363 K, then decreases to $\sim$1 Hz at 433 K. Fig. 5(b) shows the thermal variation of the real part of the complex conductivity, σ', extracted from the frequency-independent region at 10 mHz. At this frequency, σ' can be assimilated to the dc conductivity. The dc conductivity is strongly activated up to *ca.* 360 K, next starts to decrease slowly up to 415 K and then exhibits an abrupt drop. All other heating and cooling cycles follow a common trace that differs significantly from the first heating curve. Notably, the electrical conductivity (at a given temperature) is smaller by three orders of magnitude when compared to the first heating curve and displays no discontinuities. The conductivity data can be clearly correlated with the magnetic behavior. When the temperature increases, the conductivity of the LS form also increases, but above *ca.* 360 K, the LS $\rightarrow$ HS crossover counterbalances the effect of the thermal activation, which means that the HS form of **1** is more insulating than the LS form. Around 415 K, an irreversible transition occurs towards the thermodynamically stable form, in agreement with the magnetic and optical observations. This stable phase is significantly more insulating than the "as-prepared" sample, but the LS form also exhibits a higher conductivity than the HS form (at a given temperature). As far as the charge

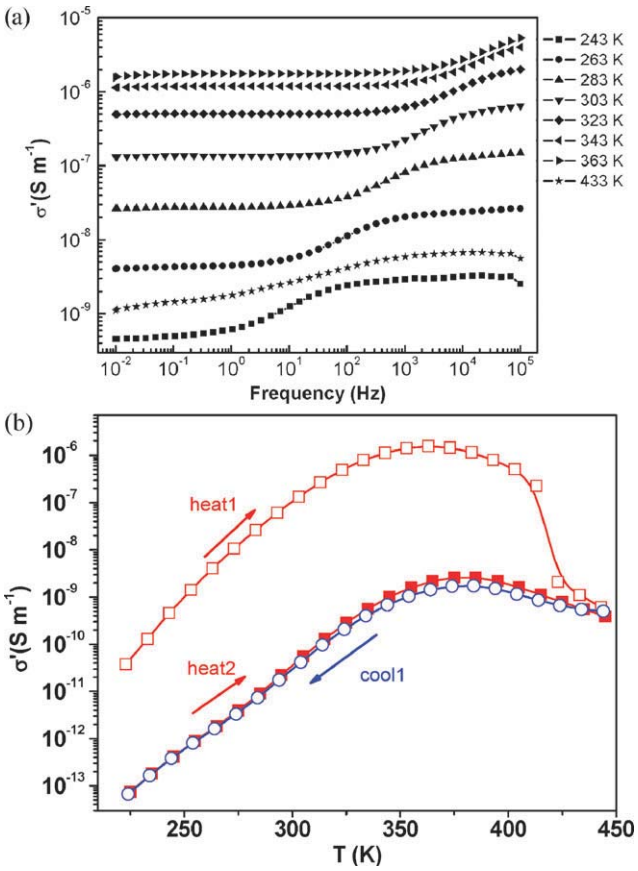

Fig. 5 (a) The frequency dependence of the ac conductivity of **1** recorded at selected temperatures between 243 and 433 K during the first heating cycle. (b) The temperature dependence of the ac conductivity of **1** (recorded at 10 mHz) after two successive thermal cycles (first cycle: open symbols, second cycle: closed symbols).

transport mechanism is concerned, in such a low mobility solid, the conductivity should be associated with a charge-hopping process. The fact that f_c exhibits a similar temperature dependence as the ac conductivity strongly suggests that this frequency corresponds to the hopping frequency.[16] These processes can be straightforwardly analyzed within the Jonscher or electric modulus formalisms,[17] but such a detailed study is out of the scope of the present paper and the work will be published elsewhere.

The various physical property measurements (magnetic, optical and electric) corroborate the occurrence of an irreversible transition in **1** during the first heating cycle. However, our visual observations reveal that this transition is followed by a recrystallization of the sample at higher temperatures. This finding suggests that the change of the thermal spin crossover curve from a rather abrupt to a gradual one is not driven by a self-grinding process. Indeed, such an irreversible transition may also be explained by thermal degradation or by polymorphism. In the latter scenario, it is assumed that the as-prepared metastable polymorph is converted to the thermodynamically stable polymorph during the first heating process. In order to assess the validity of these hypotheses, we have carried out different thermal and crystallographic analyses on **1**.

Thermal analysis

The DSC curves of a powder sample between 300 and 450 K are shown in Fig. 6. Two heating–cooling sequences were carried out; the first heating mode reveals a very broad endothermic peak corresponding to the gradual spin crossover phenomenon between *ca.* 340 and 410 K, and a subsequent well-defined endothermic peak around 439 K. The onset of the transition occurring at 430 K corresponds to the abrupt and irreversible change observed in the physical properties. Conversely, in the cooling mode, the DSC curve reveals a single very broad exothermic peak corresponding to the spin conversion from the HS to the LS state. The same broad peak is observed during the second heating–cooling cycle, but without the anomaly observed during the first heating. A simultaneous DTA-TG analysis (Fig. 7) clearly confirms that no mass change is associated with this endotherm. On the other hand, above 480 K, the DTA-TG analysis shows a reduction of sample mass, which corresponds to the beginning of the sublimation of the sample.

Crystal structures

Oliver *et al.*[18a] and other groups[18b,c] have described the room temperature (LS) structure of **1**, but to our knowledge, no other polymorphs have been published until now. The crystal structures of a freshly obtained $[Fe(HB(pz)_3)_2]$ single-crystal were resolved by X-ray crystallography at 298 K (LS state) and 420 K (LS + HS mixture) (Fig. 8 and Table 1). The X-ray analysis did not reveal any change in space group over the temperature range 298–420 K. Both structures belong to the monoclinic space group $P2_1/n$ ($Z = 4$). The symmetry of the molecule in the solid state is virtually D_{3d}, and the $[FeN_6]$ octahedral coordination sphere is formed of six nitrogen atoms belonging to the pyrazolyl ligands. Selected bond lengths and angles are given in Table 2 and Table 3,

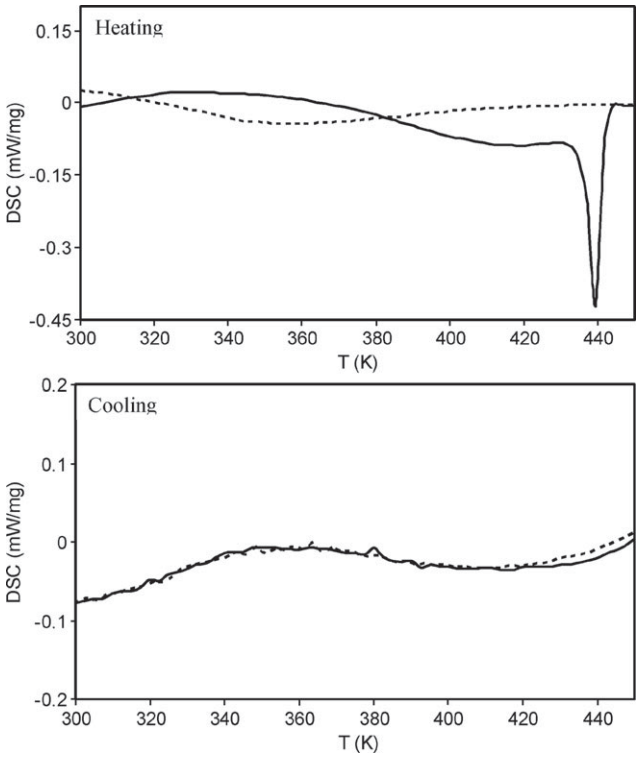

Fig. 6 DSC curves of **1** recorded in heating and cooling modes (two successive cycles; first cycle: full lines, second cycle: dashed lines).

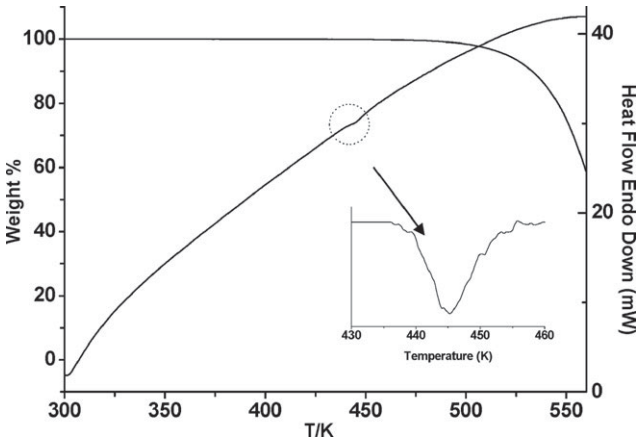

Fig. 7 Simultaneous DTA-TG curves of **1** in the first heating sequence.

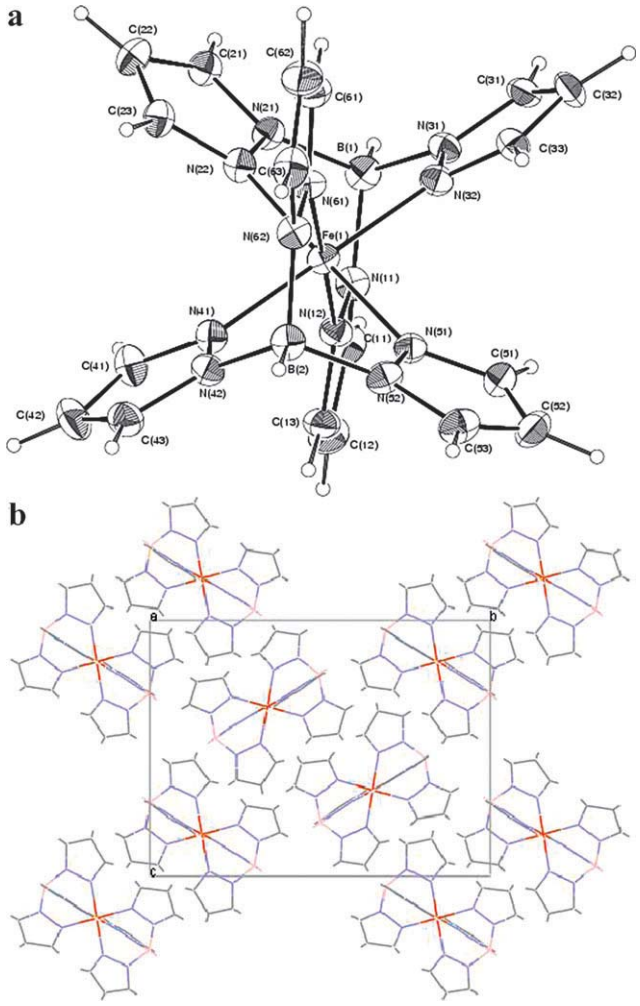

Fig. 8 a: An ORTEP view of the $Fe[HB(pz)_3]_2$ molecule (ellipsoids are drawn at the 50% probability level). b: The crystal packing at 298 K.

Table 2 Selected bond lengths (Å) for **1**

	T = 180 K	T = 298 K	T = 420 K
Fe(1)–N(12)	1.9774(17)	1.980(3)	2.095(4)
Fe(1)–N(22)	1.9871(17)	1.987(3)	2.097(3)
Fe(1)–N(32)	1.9789(16)	1.980(4)	2.099(5)
Fe(1)–N(41)	1.9800(16)	1.974(4)	2.091(5)
Fe(1)–N(51)	1.9833(16)	1.992(3)	2.113(3)
Fe(1)–N(61)	1.9770(16)	1.976(3)	2.094(4)

respectively (see ESI for further XRD data†). Since a change from the t_{2g}^6 LS state to the $t_{2g}^4e_g^2$ HS state is predicted to be accompanied by an expansion of the metal–ligand bond lengths from *ca.* 2.0 to 2.2 Å, accurate X-ray crystal analyses provide useful indications of the spin state of the iron(II) ion. In compound **1**, each Fe–N bond is lengthened by approximately 5.5–6% upon increasing the temperature, the average Fe–N distances at 298 K and 420 K being 1.982(8) and 2.098(10) Å, respectively. The high temperature (420 K) values correspond to a *ca.* 1 : 1 mixture of HS and LS states, in reasonably good agreement with the magnetic data. Considering the unit cell parameters, as might be expected, the cell volume increases with temperature due to the combined effect of thermal dilatation and spin state change. This increase is accompanied by a rise in the value of the *b* and *c* parameters, whereas the *a* value decreases slightly (Table 4). Depending on the temperature, the bond angles around the nitrogen atoms bonded to the boron atoms do not vary in the same way; some of them decrease whereas others increase. It is worth noting that while the N–N–C angles do not change, the N–N–B angles increase slightly and the C–N–B angles decrease by about 1.5% between 298 to 420 K. This change is consistent with the variation in the Fe–B bond lengths; Fe–B2: 3.085 Å at 298 K and 3.154 Å at 420 K. Finally, an important point is that above *ca.* 420 K, the crystals systematically broke apart, in agreement with the observations of Grandjean *et al.*[5] This can be explained by the loss of cohesion upon increasing the temperature due to the rise in the free volume of the unit cell.

These XRD results indicate a polymorph form of the crystal, in comparison with the results of Oliver *et al.*,[18a] who determined at 289 K a different unit cell, characterized by a volume of 2240.3 Å^3, which is significantly higher than the volume of 2181.0(3) Å^3 obtained by us at 298 K. At this

Table 3 Selected bond angles (°) for **1**

	T = 180 K	T = 298 K	T = 420 K
N(12)–Fe(1)–N(22)	89.24(7)	88.33(11)	86.53(14)
N(12)–Fe(1)–N(32)	87.77(7)	89.05(12)	86.34(15)
N(12)–Fe(1)–N(41)	91.72(7)	91.67(12)	92.67(15)
N(12)–Fe(1)–N(51)	92.41(7)	92.68(11)	94.62(14)
N(12)–Fe(1)–N(61)	179.09(7)	179.01(12)	177.96(16)
N(22)–Fe(1)–N(32)	88.15(7)	88.35(12)	86.11(12)
N(22)–Fe(1)–N(41)	92.73(7)	92.25(12)	96.01(14)
N(22)–Fe(1)–N(51)	178.14(7)	177.97(12)	177.13(12)
N(22)–Fe(1)–N(61)	90.18(7)	90.88(11)	92.37(14)
N(32)–Fe(1)–N(41)	178.98(7)	179.07(13)	177.60(14)
N(32)–Fe(1)–N(51)	91.06(7)	89.91(12)	91.33(12)
N(32)–Fe(1)–N(61)	91.51(7)	91.53(12)	95.30(15)
N(41)–Fe(1)–N(51)	88.07(7)	89.48(12)	86.57(14)
N(41)–Fe(1)–N(61)	89.01(7)	87.75(12)	85.74(15)
N(51)–Fe(1)–N(61)	88.16(7)	88.12(11)	86.56(14)

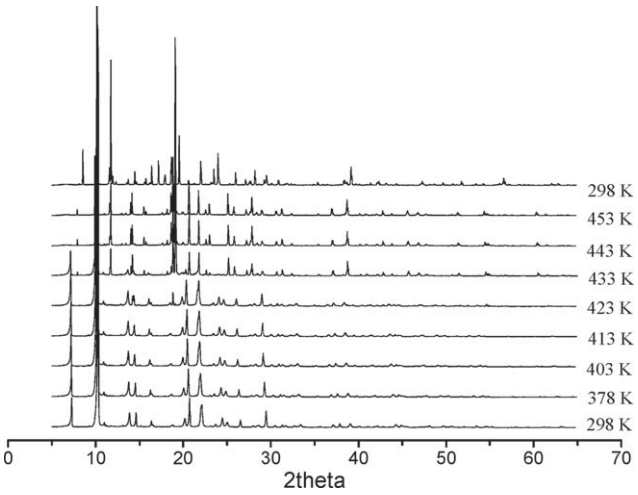

Fig. 9 Selected X-ray diffraction patterns of **1** acquired during the first heating sequence up to 453 K and after cooling back to room temperature (from bottom to top).

point, it is worth noting that polymorphism in connection with SCO phenomena has already been observed in certain pyrazolylborate complexes.[19] In order to elucidate the possible polymorphism in **1**, we recorded powder X-ray diffractograms of an "as-prepared" powder sample between room temperature and 453 K (Fig. 9). At room temperature, the lattice parameters belong to the tetragonal system with $a = b =$ 17.11(2) and c = 7.493(7) Å. Above 413 K, a phase transition clearly occurs, but up to 453 K, cell refinement was not possible due to the co-existence of at least two different phases. The variation of the cell parameters and the corresponding volume are reported in the ESI†; a gradual volume increase of *ca.* 4% between room temperature and 413 K was measured. The sample was then cooled back down to room temperature, but the observed diffraction pattern was clearly different from the initial one recorded at the same temperature. Indeed, the room temperature diffraction pattern obtained after a thermal cycle could be refined by similar lattice parameters as the single-crystals (monoclinic system; a = 9.89(1) Å, b = 17.00(2) Å, c = 12.87(1) Å, V = 2149.6(6) Å^3 and β = 96.61(1)°), and the powder diffraction pattern generated from the single-crystal data appeared to be very similar to experimentally obtained powder patterns (see ESI†). Following this heating–cooling sequence, a few single-crystals could be isolated and investigated by X-ray crystallography. The structure and space group ($P2_1/n$ (Z = 4), a = 9.900(2) Å, b = 17.020(3) Å, c = 12.890(3) Å, V = 2157.8(8) Å^3 and β = 96.53(3)°; T = 180 K) of these crystals was found to be comparable with those of crystals obtained by sublimation (see above).

These observations lead us to propose the following scenario for the thermal behavior of **1**. A freshly sublimed sample—depending on the details of the sublimation process—may consist of either a fine powder or a coarse crystalline material, which is comprised of tetragonal or monoclinic polymorphs of **1**, respectively. During the first heating sequence, the initially metastable LS tetragonal polymorph abruptly transforms to the thermodynamically stable HS monoclinic form at around 400–410 K (depending on the heating rate). If the sample is

Table 4 Variation of the unit cell parameters of a single-crystal of **1** during the first heating process

T/K	298	323	343	363	383	403	423	Variation
a/Å	9.9287(7)	9.9239(6)	9.9031(8)	9.8737(8)	9.8457(9)	9.8311(7)	9.8158(8)	−1.137%
b/Å	17.1099(16)	17.1801(13)	17.3099(14)	17.4477(15)	17.5817(15)	17.6930(14)	17.7404(15)	+3.685%
c/Å	12.9531(14)	13.0020(12)	13.0885(12)	13.1787(13)	13.2708(12)	13.3407(13)	13.4235(14)	+3.631%
β (°)	96.605(6)	96.646(6)	96.773(7)	96.927(7)	97.012(6)	97.117(6)	97.381(7)	+0.803%
V/Å^3	2185.9(7)	2201.1(5)	2227.99(4)	2253.77(3)	2280.05(4)	2302.61(3)	2318.11(5)	+6.048%

allowed to stand at high temperature (*ca*. 420–430 K) for several minutes, rather large single-crystals of this monoclinic polymorph can be grown. These crystals display the same structure as single-crystals obtained directly after sublimation. Apparently, this crystal growth occurs at the onset of sublimation of the sample. During successive cooling and heating cycles, the compound preserves its monoclinic structure, and LS to HS conversion gradually takes place in this lattice between room temperature and 450 K. However, around 420 K, the crystals break apart, presumably due to large lattice strains; this phenomenon does not significantly influence the material's physical properties. As a perspective, it would certainly be very interesting to solve the structure of the tetragonal polymorph from high quality powder XRD data in order to search for correlations between the crystal structure and the magnetic behavior of the two polymorphs, alongside the ideas proposed by Reger *et al.*[20]

4. Conclusions

In this work, we have re-investigated the remarkable spin crossover properties of the complex $[Fe(HB(pz)_3)_2]$. For the most part, we have confirmed the observations previously published in the literature. However, our results do not support the proposition of Grandjean *et al.*,[5] who explained the irreversibility of the abrupt spin transition observed during the first heating sequence as a self-grinding process. Our novel structural data reveal a rich polymorphism in this compound, and, on the basis of these findings, we propose a new interpretation of its magnetic behavior. In particular, we have associated the irreversible transition with a structural change between a metastable tetragonal and a stable monoclinic form. Additionally, we have revealed that solid $[Fe(HB(pz)_3)_2]$ exhibits an electrical conductivity that is moderate on an absolute scale but relatively high within the family of spin crossover complexes. Even more importantly, the conductivity changes by 3–4 orders of magnitude when the material passes through the first (irreversible) transition. This property, together with the knowledge that this thermochromic compound is stable to light, air and water, as well as the fact that it can be deposited on surfaces by sublimation, suggests that it might be useful as an active element in ROM-type devices for various applications, alongside the initial ideas of Kahn and Martinez.[21]

Acknowledgements

The authors are grateful to L. Vendrier, L. Rechignat, J.-F. Meunier (LCC) and J. Jaud (CEMES) for technical assistance. This work was financially supported by the ANR NANOMOL project.

References

1 S. Trofimenko, *Scorpionates: The Coordination Chemistry of Polypyrazolylborate Ligands*, Imperial College Press, London, UK, 1999.
2 G. J. Long, F. Grandjean and D. L. Reger, *Top. Curr. Chem.*, 2004, **233**, 91.
3 J. P. Jesson, J. F. Weiher and S. Trofimenko, *J. Chem. Phys.*, 1968, **48**, 2058.
4 B. Hutchinson, L. Daniels, E. Henderson, P. Neill, G. J. Long and L. W. Becker, *J. Chem. Soc., Chem. Commun.*, 1979, 1003.
5 F. Grandjean, G. J. Long, B. B. Hutchinson, L. Ohlhausen, P. Neill and J. D. Holcomb, *Inorg. Chem.*, 1989, **28**, 4406.
6 M. S. Haddad, W. D. Federer, M. W. Lynch and D. N. Hendrickson, *J. Am. Chem. Soc.*, 1980, **102**, 1468.
7 E. W. Müller, H. Spiering and P. Gütlich, *J. Chem. Phys.*, 1983, **79**, 1439.
8 P. Gütlich, A. Hauser and H. Spiering, *Angew. Chem., Int. Ed. Engl.*, 1994, **33**, 2024.
9 Y. Miyazaki, T. Nakamoto, S. Ikeuchi, K. Saito, A. Inaba, M. Sorai, T. Tojo, T. Atake, G. S. Matouzenko, S. Zein and S. A. Borshch, *J. Phys. Chem. B*, 2007, **111**, 12508.
10 S. Trofimenko, *J. Am. Chem. Soc.*, 1967, **89**, 3170.
11 P. T. Beurskens, G. Admiraal, G. Beurskens, W. P. Bosman, S. García-Granda, R. O. Gould, J. M. M. Smits and C. Smykalla, *The DIRDIF Program System*, University of Nijmegen, The Netherlands, 1992.
12 G. M. Sheldrick, *SHELXS-97, Program for the solution of crystal structures*, University of Göttingen, Germany, 1997.
13 A. L. Spek, *PLATON: A Multipurpose Crystallographic Tool*, Utrecht University, The Netherlands, 1998.
14 J. P. Jesson, S. Trofimenko and D. R. Eaton, *J. Am. Chem. Soc.*, 1967, **89**, 3158.
15 A. Bousseksou, G. Molnár, P. Demont and J. Menegotto, *J. Mater. Chem.*, 2003, **13**, 2069.
16 J. C. Dyre and T. B. Schroder, *Rev. Mod. Phys.*, 2000, **72**, 873.
17 A. K. Jonscher, *Dielectric Relaxation in Solids*, Chelsea Dielectric Press, London, UK, 1983.
18 (*a*) J. D. Oliver, D. F. Mullica, B. B. Hutchinson and W. O. Milligan, *Inorg. Chem.*, 1980, **19**, 165; (*b*) F. R. Fronczek, 2006, private communication; (*c*) Y.-H. Xing, K. Aoki and F.-Y. Bai, *Chem. Res. Chin. Univ.*, 2005, **21**, 396.
19 D. L. Reger, J. R. Gardinier, M. D. Smith, A. M. Shahin, G. J. Long, L. Rebbouh and F. Grandjean, *Inorg. Chem.*, 2005, **44**, 1852.
20 D. L. Reger, J. R. Gardinier, J. D. Elgin, M. D. Smith, D. Hautot, G. J. Long and F. Grandjean, *Inorg. Chem.*, 2006, **45**, 8862.
21 O. Kahn and C. J. Martinez, *Science*, 1998, **279**, 44.